Surface Structure of Nafion in Vapor and Liquid

Maria Bass,[†,‡] Amir Berman,[§] Amarjeet Singh,[∥] Oleg Konovalov,[∥] and Viatcheslav Freger*[,†,‡,§]

Zuckerberg Institute for Water Research, Unit of Environmental Engineering, and Department of Biotechnology Engineering, Ben-Gurion University of the Negev, P.O. Box 635, Beer-Sheva 84105, Israel, and European Synchrotron Radiation Facility, ID10B, 6 Rue Jules Horowitz, BP-220, 38043 Grenoble CEDEX, France

Received: November 29, 2009; Revised Manuscript Received: February 8, 2010

The microstructure of Nafion varies in response to changes in hydration. Thus, it undergoes a transition from tightly packed bundles of inverted micelles with aqueous cores and fused hydrophobic shells ("macaroni bundles") at low hydrations to normal type ("spaghetti") micelles at high hydrations. It was postulated recently that a similar "macaroni−spaghetti" transition, i.e., breakup of surface-aligned macaroni to randomly oriented spaghetti, takes place at the polymer surface when the external medium is changed from vapor to liquid water, which can explain some puzzling features of Nafion and similar microphase-separated ionomers. The resulting (nonequilibrium) structures may remain confined to a few nanometers thick surface region. Here, this picture is corroborated using grazing-incidence small-angle X-ray scattering (GISAXS), contact angle, and atomic force microscopy (AFM). The enhanced alignment of bundles adjacent to the surface in vapor, similar to the effect of biaxial stretching, is elucidated by GISAXS of spin-cast Nafion films. It is inferred from the characteristic change in relative intensities and position of the ionomer peak in the $X-Y$ (in-plane) and Z (out-of-plane) directions with varying X-ray penetration depths into the film. However, contact angle measurements show that the relatively smooth and very hydrophobic surface of Nafion in vapor transforms to a hydrophilic surface, when vapor as the external medium is replaced with liquid water. In addition, AFM indicates that the surface roughness significantly increases in liquid. The results demonstrate that the surface region of Nafion and similar microphase-separated materials may be indeed subject to drastic structural variations, even though the extremely slow relaxation of the solid matrix may preclude propagation of such changes into the bulk. These effects may have a profound effect on the macroscopic characteristics of Nafion membranes, such as hydration and conductivity, as well as their functioning as ion-selective barriers in electrochemical and other applications.

1. Introduction

Nafion, a perfluorinated ionomer containing negatively charged sulfonic groups, has attracted much attention due to its importance as a proton-conducting membrane material for fuel cells and other electrochemical applications.[1–8] It owes its excellent chemical stability and ionic conductivity to the Teflon-like hydrophobic backbone and highly hydrophilic ionizable sulfonic groups (Figure 1), as well as the unique microphase-separated structure composed of elongated (2D) micelles.[9–14] The microstructure of Nafion profoundly affects its hydration and conductivity, the characteristics crucial for its functioning as an ion-selective barrier.

Hydration of Nafion is determined by the balance between the osmotic pressure due to sulfonic groups, elastic pressure due to viscoelastic deformation of the matrix, and a special type of interfacial Laplace pressure exerted on the water microphase. The latter arises from the interplay between the interfacial energy and the so-called corona stretching of polymer chains adjacent to the intrapolymer microscopic interface, which stabilizes the microphase-separated structure.[15] This pressure is always finite unless the hydration becomes infinite, i.e., Nafion dissolves. The interfacial area and total interfacial energy are closely related to the microstructure, which has been thoroughly studied over the last decades.[9–14]

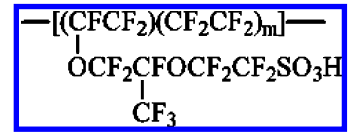

Figure 1. The chemical structure of Nafion 117, $m = 6.5$.[3]

On the basis of analysis of scattering and other data, Schmidt-Rohr and Chen[14] recently concluded that hydrated solid Nafion assumes a 2D microstructure, whereby the polar microphase composed of aggregated and hydrated ionic groups exists as long nanochannels embedded in a continuous matrix stitched together by entangled backbone chains and crystallites. At the nanoscale, the nanochannels are aligned within larger domains, typically >80 nm long and about 50 nm wide; however, at larger scales, the individual domains are nearly randomly oriented unless a preferential orientation is induced during film manufacturing.[13,14] Such domains may be alternatively viewed as bundles of coaligned inverted micelles of the "macaroni" shape, in which the bore space is filled with the aqueous microphase and the hydrophobic shells are fused and form a continuous matrix, as sketched in Figure 2a and b. This picture came to correct the previous one by Rubatat et al.[11,12,16] who postulated a 2D morphology of solid Nafion, but of the opposite,

* To whom correspondence should be addressed. E-mail: vfreger@bgu.ac.il.
† Zuckerberg Institute for Water Research, Ben-Gurion University of the Negev.
‡ Unit of Environmental Engineering, Ben-Gurion University of the Negev.
§ Department of Biotechnology Engineering, Ben-Gurion University of the Negev.
∥ European Synchrotron Radiation Facility.

10.1021/jp9113128
Published on Web 03/01/2010

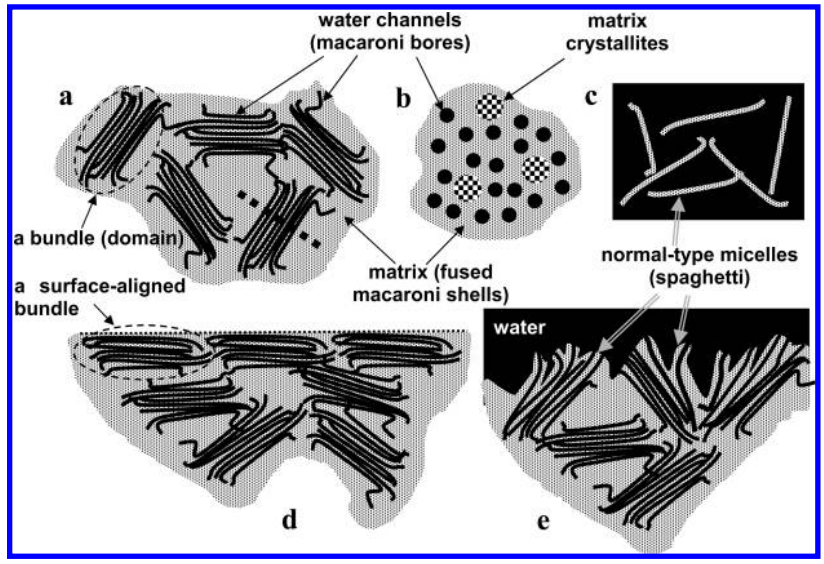

Figure 2. Schematic representation of the bulk and surface structure of Nafion in various environments: (a) the bulk Nafion composed of randomly oriented bundles of inverted micelles ("macaroni"), black solid lines showing water-filled nanochannels;[14] (b) the cross section of a bundle along the thick dotted line in part a showing water-filled channels;[14] (c) normal rod-like micelles ("spaghetti") of Nafion in a dilute solution;[9] (d) arrangement of aligned bundles near the vapor−polymer surface; (e) roughening of the Nafion surface in liquid water accompanied by random misalignment and break-up of bundles to "spaghetti". Black color designates the aqueous phase, gray color the matrix, and checkered pattern the matrix crystallites.

"spaghetti", type, i.e., normal-type micelles with a Teflon-like core. Presently, both groups seem to agree that the nanochannel morphology more adequately describes the microstructure of moderately hydrated solid Nafion.[8] However, as is well-known,[9,10] when hydration increases, Nafion should inevitably undergo at some point a transition whereby the micelle structure is inverted and "macaroni" bundles break up and form entangled and, ultimately, dispersed "spaghetti", as schematically shown in Figure 2c. A similar conclusion follows from a simple analysis based on the minimum of total interfacial energy.[15]

The characteristic lateral dimension of either type of micelles shows up as the ionomer peak in SAXS and SANS spectra of solid Nafion and its solutions. In either case, the 2D structures are rigid and stable owing to long crystallites formed from tightly packed backbone chains (see Figure 2b).[13,14] The crystallites are thermodynamically favored in the dry state and may survive virtually infinitely at ambient temperatures, serving as transient physical cross-links. This results in extremely slow bulk relaxation, on the time scale of months and years, in response to swelling[17] or mechanical[18] stresses. As pointed out by Benziger et al.,[17,19] the relaxation of Nafion matrix is much slower than diffusion of water to hydrophilic sites, which entails unusual behavior in terms of water sorption and diffusion. Perhaps the most controversial one is so-called Schroeder's paradox, i.e., a different water uptake from water liquid and vapor.[6,7,20–32] This long-debated nonthermodynamic phenomenon apparently originates in the fact that one nearly always deals with quasi-equilibrium while considering hydrated solid Nafion. For instance, Onishi et al. demonstrated recently that at saturation the liquid- and vapor-hydrated states of solid Nafion become identical after about 1 month;[28] however, the true infinitely stable equilibrium state at saturation is apparently the dilute dispersion,[33] i.e., neither of the obtained hydrated states. Understanding such nonequilibrium states and associated (metastable) morphologies and morphological transitions may then be relevant for practical cases.

One may note that the thin external surface of Nafion is a special region. First, it involves additional tensions with the external medium, liquid or vapor; therefore, for a given (not necessarily equilibrium) hydration, it may adopt different configurations depending on the relations between these tensions. Second, the limitations imposed by relaxation are less severe than in the bulk, both because of the weaker topological constraints and the tiny distance that relaxation needs to propagate. Thus, when a solid Nafion is immersed in liquid water, the surface region tends to attain the equilibrium dissolved state, i.e., undergo the "macaroni−spaghetti" transition. Within the scale of micelle spacing, the hydrophilic groups may rapidly migrate to the surface and adopt a normal-type micelle (spaghetti) configuration; however, it may take exceedingly long to see this structure propagated to the bulk.

On the other hand, for vapor equilibration, due to a different relation between surface tensions,[33] the hydrophobic matrix may "spread" over the polymer, while the hydrophilic nanochannels "sink" below the surface. This hydrophobic surface configuration in vapor was deemed responsible for Schroeder's paradox (due to different Laplace pressures)[15] and for an additional interfacial resistance to water transport.[19,34] Obviously, *at saturation*, this morphology is unstable and the buried hydrophilic groups should eventually migrate to the surface and get covered with a flat thin film of water, which is what apparently occurred in experiments of Onishi et al.[28] However, when the surface is initially hydrophobic (e.g., by starting with a dry polymer) and condensation of water is prevented (e.g., by keeping the system slightly under saturation), the high energetic and kinetic barriers associated with condensing water on the hydrophobic surface *and* simultaneously rearranging many groups may effectively keep the polymer kinetically trapped in this state for very long.

A notable point is that the quasi-equilibrium surface in vapor has a finite tension, approximately equal to that of the perfluorinated matrix. Consequently, it is expected that in vapor the surface will tend to flatten. To keep the surface flat, the bundles adjacent to the surface will have to preferentially align in the $X-Y$ plane, as shown in Figure 2d, since misalignment will be energetically unfavorable. In contrast, in liquid, the surface tension of the relaxed polymer−liquid interface, both internal and external, is *zero*; then, misalignment of micelles or whole bundles will not cost energy and, in fact, it is expected that

entropy will encourage individual "spaghetti" micelles to stick out randomly (Figure 2e). We see that both in vapor and in liquid the structural rearrangement, intimately related to unusual properties of Nafion, may occur and remain confined to a thin surface region. The thickness of this region should be commensurable with the micelle spacing, i.e., a few nanometers, since it is within this thickness that the micelles can relatively readily reorient or disentangle. Examination using techniques that probe such a surface region and compare it with the underlying bulk may then help test the proposed structural picture of the Nafion surface. In this paper, we present some data in favor of this picture obtained using measurements of contact angle, grazing-incidence small-angle X-ray scattering (GISAXS), and atomic force microscopy (AFM).

2. Experimental Section

Nafion 117 membrane and 5% commercial solution of Nafion in a proprietary mixture of water and low alcohols and ethers were purchased from Sigma-Aldrich and used as obtained.

Grazing-Incidence SAXS. The GISAXS experiments were carried out at ESRF, Grenoble, at the ID10B beamline. The incident beam was of wavelength $\lambda = 1.54$ Å (8 keV). The sample was either a 10 mm wide and about 3 cm long piece of Nafion membrane pulled taut over the flat top of a stainless still block using a clamp or a film of Nafion spin-coated on an about 15×15 mm^2 large piece of a Si wafer. The spin-coated samples were prepared using an EC 101 spin-coater (Headway Research, Inc., Garland, TX) at a rotation speed of 4000 rpm from a 5% Nafion solution and then annealed at 200 °C overnight. The thickness of the Nafion film (100 ± 6 nm) was determined using a spectroscopic ellipsometer (Sentec, Germany).

In scattering experiments, the sample was mounted horizontally inside a temperature and humidity controlled chamber equipped with X-ray transparent Kapton windows. GISAXS spectra were recorded using a vertical position sensitive detector (PSD), scanning the 2θ angle in the horizontal $X-Y$ direction (parallel to the sample surface). Reported measurements in this study were performed at 30 °C. The relative humidity inside the chamber was maintained close to saturation (>84%) by having inside the chamber a small water reservoir with a separate temperature control that was kept slightly below 30 °C to prevent condensation. Prior to measurements, the samples were pre-equilibrated in a vapor atmosphere at 84% relative humidity in a separate closed and evacuated vessel for at least 4 days, rapidly transferred to the chamber, and left to re-equilibrate for at least 1 h. There was no indication that the samples could be distorted or their flatness affected during equilibration, and they could be successfully aligned using the standard procedure. In order to minimize radiation damage, the sample was translated laterally by about 1 mm perpendicular to the beam direction and realigned for each incident angle.

The GISAXS spectra were recorded at several incidence angles α_i, below, above, and near the critical angle α_c that was estimated using the formula[35]

$$\alpha_c = \lambda\sqrt{\rho_e r_e/\pi} \quad (1)$$

where $r_e = 2.8 \times 10^{-15}$ m is the classic radius of an electron and ρ_e is the electron density calculated from the known density (2.0 g/cm^3 for dry polymer), chemical formula (Figure 1), and equivalent weight (1100 g/mol) that sets $m = 6.5$ in Figure 1.[3] The calculated critical angle of the H-form of Nafion varies from 0.20° for dry polymer to 0.185° for equilibrium with saturated vapor (14 water molecules per sulfonic group[7]). Since the Nafion surface in vapor is enriched in perfluorinated polymer,[15,36–38] the actual value of α_c is likely to be closer to the upper limit and might even approach the similarly calculated critical angle 0.21° of Teflon, a close analogue of the perfluorinated matrix. X-ray reflectivity experiments, i.e., the intensity of the X-ray beam specularly reflected from the sample surface measured at varying incident angle, indeed indicated values close to 0.20−0.21°; however, accurate determination of the critical angle using this technique was difficult due to surface roughness and the proximity to the value for the underlying Si substrate (0.23°).

Contact Angle and AFM. The advancing contact angles θ were measured using an OCA-20 contact angle analyzer (Data Physics, Germany) equipped with a video camera and software for image grabbing and analysis. Using a microsyringe, a sessile drop of water about 5 μL large was placed on the top surface of a dry or vapor-equilibrated sample of Nafion membrane. In the case of liquid-equilibrated Nafion, a similarly sized air bubble was attached from below to the down-facing surface of Nafion under water (captive bubble method). The membrane was "soaked" in water for at least 16 h before running measurements. The vapor-exposed samples were pre-equilibrated for at least 4 days in closed and evacuated desiccators, and all reported angles were measured within no more than 5 min after opening the desiccator. The contact angle of a sessile drop decreases with time, since the polymer adsorbs water;[37] therefore, the reported values are the ones obtained within the first 5−10 s after placing the drop.

Topographic AFM images of the Nafion surface were obtained using a MultiMode Nanoscope III (DI-Veeco) in tapping mode in air and under water. Silicon probes (Veeco-probes) with a 125 μm long cantilever, 40 N/m nominal spring constant, and 8 nm nominal tip radius were used at their fundamental resonance frequency which typically varied from 200 to 400 kHz to image vapor-exposed Nafion. To scan the membrane under water, the NP-S10 probes with 180 μm long cantilevers and 10 nm nominal tip radius were used at 18−26 kHz resonance frequency. Samples were equilibrated for several days in the medium, under which it was scanned.

3. Results

3.1. GISAXS: Alignment of Micelles near the Vapor−Polymer Surface. Figure 3 displays the results of GISAXS experiments for spin-cast films of Nafion as the total scattered intensity I integrated over the entire PSD at several incident angles α_i versus the magnitude of the lateral (in plane) scattering vector Q_{xy}. Notably, the absolute intensity varies nonmonotonously with α_i and is the largest at $\alpha_i = 0.2°$, which is known to result from the enhancement of the intensity at $\alpha_i \approx \alpha_c$ due to interference of the incident and reflected waves, usually referred to as the Yoneda or Vineyard effect.[39,40] This offered another way of estimating α_c, which produced a value close to 0.2°, as expected for a Teflon-like surface depleted of water and ionic groups.

The ionomer peak sitting on top of a featureless scattering background is well observed in all spectra in Figure 3a as a shoulder at $Q_{xy} \approx 0.15-0.18$ Å^{-1}. However, since the background scattering exponentially decays with Q_{xy} with an exponent somewhat between 1 and 2 (see Figure 3 and ref 14), the ionomer peak could be enhanced by plotting $I \cdot Q_{xy}$ vs Q_{xy}, correcting for the high background radiation at small angles, Figure 3b. The intensity of the ionomer peak relative to the

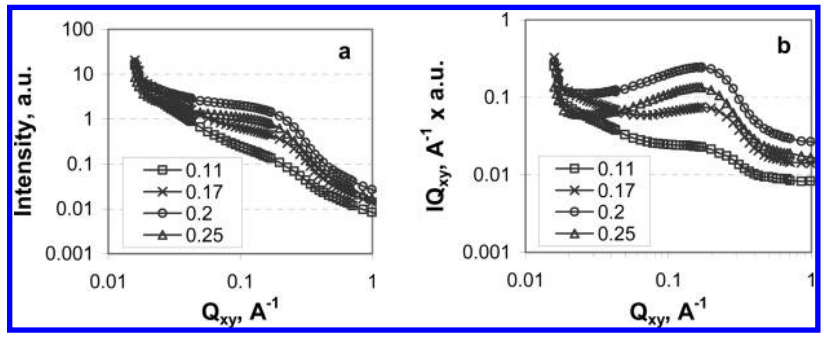

Figure 3. GISAXS intensity scattered along the surface (integrated over the Z axis) vs Q_{xy} for several incident angles: (a) I vs Q_{xy}; (b) $I \cdot Q_{xy}$ vs Q_{xy}. The sample was spin-cast film of Nafion on a Si wafer about 100 nm thick kept in a vapor close to saturation at 30°. The legends are incident angles in degrees.

background is nearly constant above and near the critical angle; however, it decreases when α_i falls well below α_c.

The amplitude of the evanescent wave at $\alpha_i < \alpha_c$ is exponentially attenuated with the depth of penetration. The characteristic attenuation depth depends on the incident angle α_i as given by the formula[41]

$$d_p = \frac{\lambda\sqrt{2}}{4\pi\alpha_c\sqrt{\sqrt{\left(\frac{\alpha_i^2}{\alpha_c^2}-1\right)^2+\frac{\beta^2}{\delta^2}}-\left(\frac{\alpha_i^2}{\alpha_c^2}-1\right)}} \approx \frac{\lambda}{4\pi\alpha_c\sqrt{1-(\alpha_i/\alpha_c)^2}} = \frac{1}{Q_c\sqrt{1-(\alpha_i/\alpha_c)^2}} \quad (2)$$

where δ and β are the scattering and absorption parts of the complex refractive index $\eta = 1 - \delta - i\beta$ and $Q_c = 4\pi\alpha_c/\lambda$ is the critical wavenumber. Calculations[13] of δ and β for the present material and conditions showed that β/δ was of the order 10^{-2}; therefore, this term could be neglected and the last approximate relation could be used. Attenuation of the ionomer peak for $\alpha_i < \alpha_c$ in Figure 3 should then be interpreted as a reduced number density of scatterers in the surface layer of a characteristic thickness of the order of d_p. Using $\alpha_i = 0.2°$, the minimal penetration depth d_{p0} at $\alpha_i \ll \alpha_c$ is $1/Q_c = \lambda/4\pi\alpha_c$, i.e., about 30−35 Å, and d_p is only 10% above this value for $\alpha_i = 0.11°$. The penetration depth at this lowest incidence angle is then commensurate with the characteristic spacing of the micelles (or water channels) in solid Nafion, which is about 40−50 Å for the vapor-equilibrated Nafion 117,[10,42] which could also be directly read from the position of the ionomer peak, 0.15−0.20 Å^{-1}. The GISAXS scattering at $\alpha_i = 0.11°$ then mostly comes from the layer of micelles immediately adjacent to the surface, for which the ionomer peak in the Q_{xy} direction appears to be appreciably attenuated. However, as α_i increases, d_p increases and becomes infinite at $\alpha_i = \alpha_c$. The observed spectra near and above the critical angle should then predominantly come from the underlying bulk and the intensity of the ionomer peak relative to the background should become independent of α_i, which is indeed observed in Figure 3.

A more detailed structural picture could be obtained from 2D scattering intensity maps that were constructed in MATLAB using the MatSpecGUI software developed by Dr. Jiři Novak, ESRF.[43] They are shown in Figure 4 for the same sample and the same incidence angles as in Figure 3. A strong anisotropy of 2D scattering pattern is observed for all values of α_i and indicates that micelle alignment spans the whole films. This is not unlikely, since the reported width (~50 nm) and length (>80 nm) of a bundle[13] are commensurate with the film thickness (100 nm) and the surface-induced alignment might well affect the whole film. It is likely that the interface with the Si substrate could also contribute to the alignment, as well as the spin-coating process, even though the sample was annealed at 200 °C.

However, even if preferential orientation of the micelles indeed occurs in the bulk, closer inspection of the GISASX maps in Figures 3 and 4 shows that the micelle alignment appears to be enhanced near the polymer−vapor interface. First, the anisotropy seems to increase as α_i decreases; i.e., the intensity of the ionomer peak in the Z direction (out-of-plane) is not attenuated as much as that of the in-plane peak. Due to this attenuation, the in-plane peak for $\alpha_i = 0.11°$ is only observable in Figure 3, where it is integrated over Z; therefore, in Figure 4, the scattering pattern for this low angle approaches that of a Bragg sheet, i.e., of a layer sitting on top of the surface. Anisotropy of the scattering pattern visibly decreases with increasing angle of incidence, and a small consistent shift of the ionomer peak along the Z axis from $Q_z \sim 0.18$ Å^{-1} at $\alpha_i = 0.11°$ to a smaller value of $Q_z \sim 0.15$ Å^{-1} at $\alpha_i = 0.25°$ is observed in Figure 4. This means that spacing of the micelles in the Z direction decreases near the surface. This is characteristic of elongated objects tending to align parallel to the surface and analogues to changes observed for bulk scattering of drawn Nafion.[16,44,45] The surface tension then produces an effect similar to biaxial stretching in the XY plane. As explained above, this pattern was expected for a vapor-equilibrated sample (Figure 2d) and indeed seems to indicate the confining and aligning effect of the polymer−vapor surface driven by its finite surface tension.

We also attempted to obtain GISAXS spectra of a genuine Nafion 117 membrane. The spectra were significantly compromised by excessive roughness of the membrane, both at micro- and macroscopic scales (see the next section), resulting in irregular diffuse scattering. Figure 5 shows a typical set of spectra for a membrane in H-form at 50% humidity (lower humidity was used, since at high humidities the membrane becomes softer and creeps upon pulling). It is seen that the ionomer peak was much obscured and at high Q_{xy} the spectrum was completely overwhelmed by the irregular scattering independent of α_i. Nevertheless, we could still observe that the ionomer peak at $Q_{xy} \sim 0.15-0.20$ Å^{-1} was more attenuated at the low incident angles, similar to Figure 3.

3.2. Contact Angle: Surface Hydrophilicity in Vapor and Liquid. Using the sessile drop and captive bubble methods, we measured the contact angles between the Nafion, water, and vapor (air) phases in vapor and in liquid, respectively, and thus observed variations of surface hydrophilicity/hydrophobicity. Figure 6 shows a typical droplet and bubble, and the contact

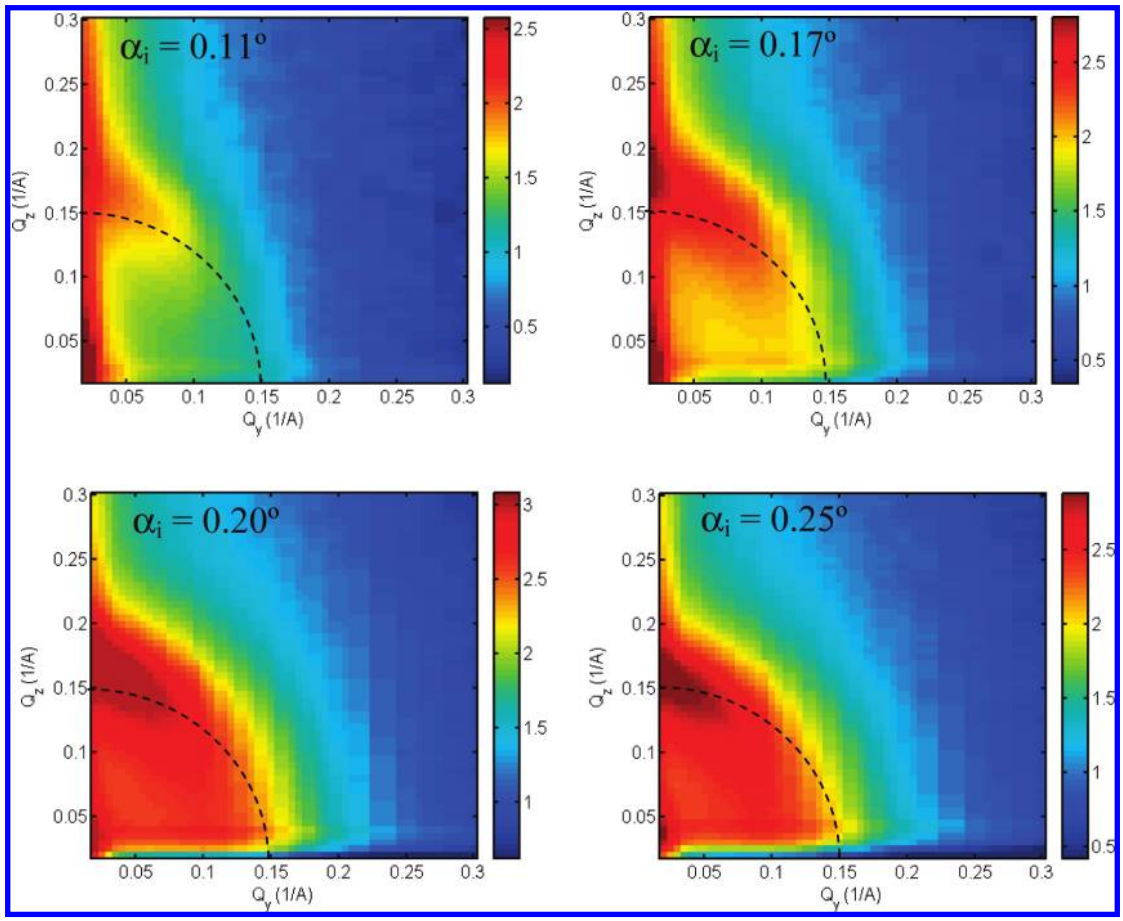

Figure 4. 2D scattering intensity maps for the 1D spectra shown in Figure 3. To facilitate comparison, the color scale for each sample is rigidly shifted by the ratio of the background intensities at $Q_{xy} = 1$ Å^{-1} in the 1D spectra. Dashed arcs at $Q_{total} = (Q_z^2 + Q_{xy}^2)^{1/2} = 0.15$ Å^{-1} are added to visualize the anisotropy of the scattering pattern and the gradual shift of the out-of-plane ionomer peak with α_i.

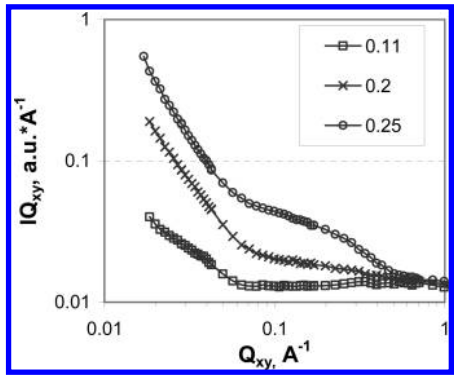

Figure 5. $I \cdot Q_{xy}$ vs Q_{xy} for a Nafion 117 membrane (H form) at several incident angles (in degrees) at relative humidity 50% and 30 °C.

angle results for Nafion membranes are summarized in Table 1 for different ionic forms that all show similar behavior. The Nafion surface in vapor appears to remain hydrophobic even in contact with nearly saturated water vapor of relative humidity 97%. Furthermore, the advancing contact angles for nearly saturated conditions were only slightly smaller than those of completely dry membranes. This is fully consistent with earlier observations.[36,38] However, the surface of a Nafion membrane immersed in pure water was hydrophilic and showed much smaller though still finite contact angles. Similar observation was made by Goswami et al. based on dynamic contact angle measurements.[37] This change is consistent with what is expected for the (probably, incomplete) "macaroni−spaghetti" transitions, i.e., inversion of micelle configuration, at the surface.

It is instructive to express the observed contact angles as the hydrophilic surface fraction f_1 by assuming that the Nafion surface is a random mosaic composed of water-like (phase 1) and Teflon-like (phase 2) patches. For this purpose, we could employ a relation that combines the Young and Cassie−Baxter equations.[46,47]

$$f_1 = \frac{\gamma_{aw}\cos\theta - (\gamma_{2a} - \gamma_{2w})}{\gamma_{1a} - \gamma_{1w} - (\gamma_{2a} - \gamma_{2w})} \quad (3)$$

where γ's are the interfacial tensions between different phases and subscripts "1", "2", "a", and "w" designate phase 1, phase 2, air (vapor), and water, respectively. Using the values for water and Teflon $\gamma_{1a} \approx \gamma_{aw} = 73$ mN/m, $\gamma_{1w} = 0$, $\gamma_{2a} \approx 19$ mN/m,[48] $\gamma_{2w} \approx 46$ mN/m,[47] eq 3 yields a low hydrophilic fraction in vapor ($f_1 \leq 0.25$) or dry state ($f_1 \leq 0.19$), irrespective of hydration, and a high one ($f_1 \geq 0.92$) under water for all ionic forms of Nafion. Note that the hydrophilic surface patches in liquid should indeed have zero tension with water, however, their tension with vapor is not necessarily identical to. For this reason, these estimates of f_1 can only be taken as rough indicators of actual surface composition.

3.3. AFM: Roughening of the Nafion Surface under Water. As discussed above, due to alignment of micelle bundles, the vapor-exposed Nafion surface gets flatter and the surface energy is minimized (Figure 2d). On the other hand, the polymer surface tension vanishes under water following "macaroni−spaghetti" transition and, in the absence of surface

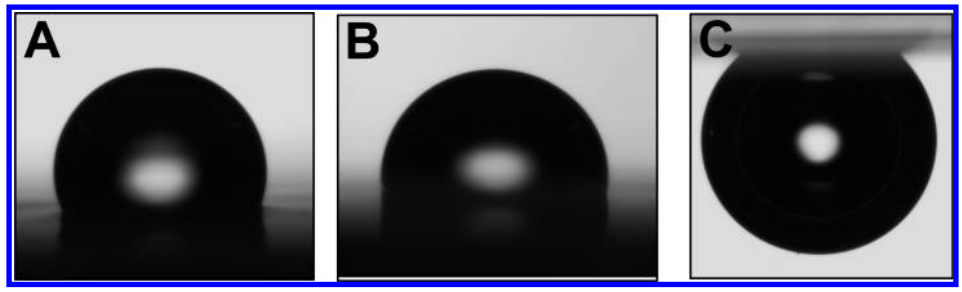

Figure 6. Water droplets in air on a Nafion membrane, dry (A) and equilibrated at 97% relative humidity (B), and an air bubble attached from below to a Nafion membrane in water (C). The volume of the droplets and bubble is 5 μL.

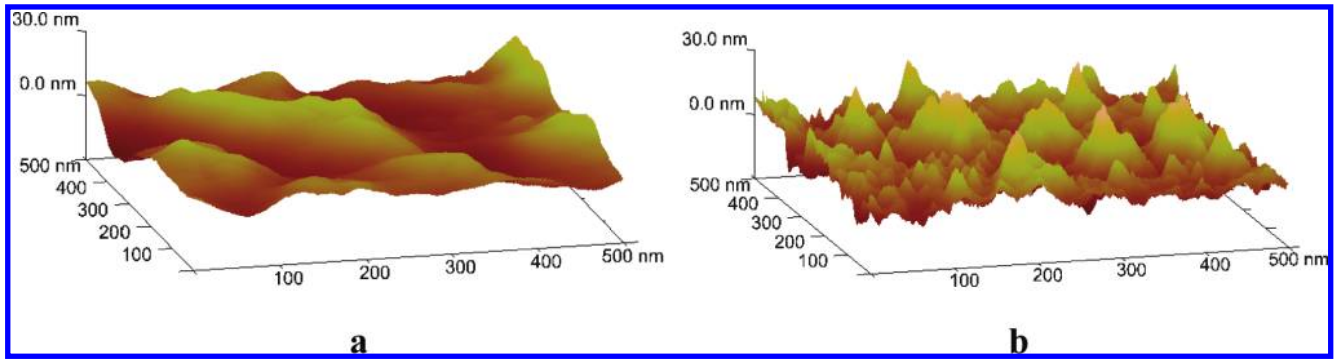

Figure 7. Surface topography of Nafion 117 membrane in H^+ form measured by AFM: (a) in air; (b) under water.

TABLE 1: The Hydration and Advancing Contact Angles Measured for Nafion 117 Membrane in Different Ionic Forms and Equilibration Conditions

	in water			in vapor, humidity 97%			dry polymer	
ionic form	h^a	θ^b	$f_1{}^c$	h^a	θ^b	$f_1{}^c$	θ^b	$f_1{}^c$
Nafion−H	22[d]	22.3 ± 0.5	0.95	12[d]	103.4 ± 1.0	0.11	108.1 ± 0.7	0.05
Nafion−Na	19.8[e]	27.5 ± 0.9	0.92	6.6[e]	92.2 ± 1.2	0.25	98.0 ± 1.2	0.17
Nafion−Li	24[e]	25.4 ± 0.3	0.93	9.1[e]	94.5 ± 1.1	0.22	96.4 ± 1.2	0.19

[a] h is the hydration expressed as the number of water molecules per sulfonic group. [b] Advancing water contact angle. [c] Hydrophilic surface fraction (eq 3). [d] Reference 7. [e] Reference 30.

tension penalty, the entropy is expected to destabilize the flat topography and promote a random reorientation of separate spaghetti, as schematically shown in Figure 2e.

The GISAXS setup used in the present study could not be used to confirm the occurrence of the above transition in liquid water. Nevertheless, topographic AFM images shown in Figure 7 may serve as an indication of the changes occurring upon exposure to water. It is observed that the vapor-exposed sample has a significantly flatter topography compared to samples exposed to liquid water. Notably, no such drastic changes occur in the bulk of Nafion at ambient temperature apart from about 50% increase in water uptake. The destabilization of the external surface may then be viewed as the very first stage of the dissolution in water, which cannot significantly advance into the bulk, since the matrix relaxation and micelle disentanglement are very slow at ambient conditions.

Interestingly, liquid methanol as an external medium was reported to have a flattening effect on the Nafion surface, similar to that of vapor.[49] Presumably, the interfacial tension between methanol and ionic aggregates exceeds the one between methanol and matrix, similar to corresponding tensions for air or vapor (cf. eq 3), which promotes "spreading" of matrix and "sinking" of ionic aggregates below the surface, similar to the effect of vapor equilibration. In contrast, subsequent transfer to liquid water was reported to produce a roughening effect,[49] similar to that observed in the present study.

Conclusions

The results obtained using the three surface sensitive techniques conform to the proposed structural picture of the thin surface layer of Nafion, whose thickness is commensurate with the characteristic spacing of micelles. In contact with water vapor, the bundles of fused inverted micelles ("macaroni") tend to align in the surface plane and bury the hydrophilic core under a thin hydrophobic shell to minimize the surface energy. This particular arrangement could be inferred from results obtained by GISAXS (preferential alignment of micelles near the surface), contact angle measurements (surface hydrophobicity), and AFM (relatively smooth surface topography). In contrast, under water, the contact angle drops drastically, indicating transformation to a hydrophilic surface, and AFM shows that the surface becomes rougher. These changes are consistent with the conclusion that the surface under water breaks up to separate spaghetti-like micelles having a zero surface tension with water and thus tending to randomly protrude from the surface into water. Since the free "spaghetti" configuration is apparently the true equilibrium state of Nafion in water, this "macaroni−spaghetti" transformation at the surface may be regarded as the

initial fairly rapid stage of the extremely slow dissolution in water. Examining the structural transformations at the surface then offers insight into true equilibrium and quasi-equilibrium states and thus sheds light on many puzzling features of Nafion and similar materials, such as Schroeder's paradox.

Acknowledgment. This work was supported by Israeli Science Foundation (Grant No. 340/04) and ESRF. The authors are grateful to Dr. Jiři Novak for help with the MatSpecGUI software, to Jürgen Jopp for help with preparation and characterization of spin-coated samples, and to Yair Kaufman for help with AFM experiments.

References and Notes

(1) *Ionomers: synthesis, structure, properties and elasticity*; Tant, M. R., Mauritz, K. A., Wilkes, G. L., Eds.; Chapman and Hall: London, 1997.
(2) *Ionomers: Characterization, Theory, and Applications*; Schlick, S., Ed.; CRC Press: Boca Raton, FL, 1996.
(3) Mauritz, K. A.; Moore, R. B. *Chem. Rev.* **2004**, *104*, 4535.
(4) Costamagna, P.; Srinivasan, S. *J. Power Sources* **2001**, *102*, 253.
(5) Perry, M. L.; Fuller, T. F. *J. Electrochem. Soc.* **2002**, *149*, S59.
(6) Broka, K.; Ekdunge, P. *J. Appl. Electrochem.* **1997**, *27*, 117.
(7) Zawodzinski, T. A.; Derouin, C.; Radzinski, S.; Sherman, R. J.; Smith, V. T.; Springer, T. E.; Gottesfeld, S. *J. Electrochem. Soc.* **1993**, *140*, 1041.
(8) Diat, O.; Gebel, G. *Nat. Mater.* **2008**, *7*, 13.
(9) Aldebert, P.; Dreyfus, B.; Gebel, G.; Nakamura, N.; Pineri, M.; Volino, F. *J. Phys.* **1988**, *49*, 2101.
(10) Gebel, G. *Polymer* **2000**, *41*, 5829.
(11) Rubatat, L.; Rollet, A. L.; Gebel, G.; Diat, O. *Macromolecules* **2002**, *35*, 4050.
(12) Rubatat, L.; Gebel, G.; Diat, O. *Macromolecules* **2004**, *37*, 7772.
(13) Gebel, G.; Diat, O. *Fuel Cells* **2005**, *5*, 261.
(14) Schmidt-Rohr, K.; Chen, Q. *Nat. Mater.* **2008**, *7*, 75.
(15) Freger, V. *J. Phys. Chem. B* **2009**, *113*, 24.
(16) Rubatat, L.; Diat, O. *Macromolecules* **2007**, *40*, 9455.
(17) Barclay Satterfield, M.; Benziger, J. B. *J. Phys. Chem. B* **2008**, *112*, 3693.
(18) Barclay Satterfield, M.; Benziger, J. B. *J. Polym. Sci., Part B: Polym. Phys.* **2009**, *47*, 11.
(19) Majsztrik, P.; Satterfielda, B.; Bocarsly, A.; Benziger, J. *J. Membr. Sci.* **2007**, *301*, 93.
(20) Schroeder, P. V. *Z. Phys. Chem.* **1903**, *45*, 75.
(21) Hinatsu, J. T.; Mizuhata, M.; Takenaka, H. *J. Electrochem. Soc.* **1994**, *141*, 1493.
(22) Cornet, N.; Gebel, G.; de Geyer, A. *J. Phys. IV* **1998**, *8*, 63.
(23) Freger, V.; Korin, E.; Wisniak, J.; Korngold, E. *J. Membr. Sci.* **2000**, *164*, 251.
(24) Choi, P. H.; Datta, R. *J. Electrochem. Soc.* **2003**, *150*, E601.
(25) Choi, P.; Jalani, N. H.; Datta, R. *J. Electrochem. Soc.* **2005**, *152*, E84.
(26) Weber, A. Z.; Newman, J. *J. Electrochem. Soc.* **2003**, *150*, A1008.
(27) Vallieres, C.; Winkelmann, D.; Roizard, D.; Favre, E.; Scharfer, P.; Kind, M. *J. Membr. Sci.* **2006**, *278*, 357.
(28) Onishi, L. M.; Prausnitz, J. M.; Newman, J. *J. Phys. Chem. B* **2007**, *111*, 10166.
(29) Elfring, G. J.; Struchtrup, H. *J. Membr. Sci.* **2007**, *297*, 190.
(30) Bass, M.; Freger, V. *Polymer* **2008**, *49*, 497.
(31) Jeck, S.; Scharfera, P.; Kinda, M. *J. Membr. Sci.* **2009**, *337*, 291.
(32) Onishi, L. M.; Prausnitz, J. M.; Newman, J. *J. Phys. Chem. B* **2007**, *111*, 10166.
(33) Freger, V. *J. Phys. Chem. B* **2009**, *113*, 24.
(34) Majsztrik, P.; Bocarsly, A.; Benziger, J. *J. Membr. Sci.* **2008**, *112*, 16280.
(35) Als-Nielsen, J.; McMorrow, D. *Elements of modern X-ray physics*; John Wiley & Sons: New York, 2001.
(36) Zawodzinski, T. A.; Gottesfeld, S.; Shoichet, S.; McCarthy, T. J. *J. Appl. Electrochem.* **1993**, *23*, 86.
(37) Goswami, S.; Klaus, S.; Benziger, J. *Langmuir* **2008**, *24*, 8627.
(38) McLean, R. S.; Doyle, M.; Sauer, B. B. *Macromolecules* **2000**, *33*, 6541.
(39) Yoneda, Y. *Phys. Rev.* **1963**, *131*, 2010.
(40) Vineyard, G. H. *Phys. Rev. B: Condens. Matter* **1982**, *26*, 4146.
(41) *X-ray and neutron reflectivity: principles and applications*; Daillant, J., Gibaud A., Eds.; Springer: Berlin, 1999.
(42) Hsu, W. Y.; Gierke, T. D. *J. Membr. Sci.* **1983**, *13*, 307.
(43) Novak, J. http://www.physics.muni.cz/~novak/MatSpecGUI/MatSpecGUI.php, Grenoble, France.
(44) Barbi, V.; Funari, S. S.; Gehrke, R.; Scharnagl, N.; Stribeck, N. *Polymer* **2003**, *44*, 4853.
(45) Van der Heijden, P. C.; Rubatat, L.; Diat, O. *Macromolecules* **2004**, *37*, 5327.
(46) Adamson, A. W. *Physical chemistry of surfaces*; Interscience Publisher, Inc.: New York, 1960.
(47) Israelachvili, J. N. *Intermolecular and Surface Forces*; Academic Press: New York, 1992.
(48) de Gennes, P. G.; Brochard-Wyart, F.; Quere, D. *Capillarity and Wetting Phenomena: Drops, Bubbles, Pearls, Waves*; Springer: New York, 2003.
(49) Affoune, A. M.; Yamada, A.; Umeda, M. *Langmuir* **2004**, *20*, 6965.

JP9113128